Journal of Crystal Growth 125 (1992) 215–222
North-Holland

JOURNAL OF CRYSTAL GROWTH

Calcium oxalate monohydrate crystallization: citrate inhibition of nucleation and growth steps

Peter A. Antinozzi, Charles M. Brown and Daniel L. Purich

Center for the Study of Urolithiasis and Pathological Calcification and Department of Biochemistry and Molecular Biology, University of Florida College of Medicine, Gainesville, Florida 32610-0247, USA

Received 30 March 1992; manuscript received in final form 29 June 1992

The inhibitory action of citrate on calcium oxalate monohydrate (COM) crystallization has been examined in terms of nucleation and crystal growth kinetic properties. Lag-time data for the appearance of crystals and [^{14}C] oxalate incorporation under crystal growth conditions allowed us to investigate the influence of citrate at physiological levels (3.5mM). Moreover, through the use of the EQUIL software, we formulated our solutions based on calculations of solute composition such that free calcium concentrations were the same in the absence and presence of this tricarboxylic acid. The presence of citrate had little effect on the apparent interfacial free energy as determined by nucleation kinetic studies, but total particle production was greater in the absence of citrate; this was evident from electron microscopy and was also indicated by corresponding values of pre-exponential terms of the Gibbs–Thomson equation. Crystal growth rates were lowered in the presence of citrate to 30% of the uninhibited value, and distinctive morphological habit modifications were also observed by scanning electron microscopy. Together, these findings suggest that citrate may influence COM crystallization at several stages, and we present a model for face-specific growth inhibition by citrate acting on the (010) COM crystal face.

1. Introduction

Understanding the factors that influence the course of calcium oxalate monohydrate (COM) crystallization promises to provide insight about processes thought important in urolithiasis. In particular, much attention has been devoted to the analysis of crystallization in terms of discretely defined physical chemical processes (i.e., nucleation, crystal growth, aggregation, and breakup) although such processes may be overlapping in a temporal sense. Nonetheless, such a physicochemical treatment may afford a means of understanding the action of agents that promote or inhibit COM crystallization. Brown et al. [1] recently described several approaches for distinguishing between crystal growth and nucleation effects, and they attempted to distinguish between the interfacial free energy term and the "nucleation efficiency" term that are related to the lag-time for crystallization by use of the Gibbs–Thomson equation. We were motivated by the success of that experimental approach to investigate the action of citrate as an inhibitor of COM crystallization. About half a century ago, Greenwald [2] first recognized the complexation of calcium ion by various organic acids, among them citrate, and he discussed the physiological significance of the sharp increase in the solubility of salts such as calcium sulfate, calcium carbonate and calcium phosphate as brought about by malic and fumaric acids. Kissen and Locks [3] established that the urinary citrate levels of patients suffering from urolithiasis were reduced compared with control subjects, and many other investigators have labored to characterize the basis for such a difference and/or its impact on crystallization. The implication that citric acid is a factor in urolithiasis promoted efforts both to understand its ability to dissolve kidney stones and its role in their formation. In 1961, Light and Zinsser [4] examined the rate of formation of

calcium oxalate in the presence of various substances found in urine, including citrate, and in fact, they studied nucleation rates by observing lag-times. Subsequent studies of the inhibitory action of citrate focused on determinations of crystal growth viewed in its broadest sense (i.e., there are many steps in the formation of a solid phase from an aqueous solution, and a substance influencing any of these steps may be called an inhibitor). For example, complexation reduces the driving force for crystal growth, and this effect must be distinguished from those that influence incorporation of lattice ions into the crystal. Even some recent crystal growth studies have overlooked this distinction [5] and experimental results represent a convolution of metal-ligand complexation and true growth inhibitory effects.

In this work, we applied nucleation kinetic [1] and crystal growth rate experiments to analyze the action of citrate on COM nucleation and crystal growth. We used the EQUIL speciation software [6] to achieve desired relative supersaturations (RS) with respect to calcium oxalate monohydrate (COM) while keeping the RSs in control solutions and citrate-containing solutions unchanged. Moreover, to minimize changes in the $[Ca^{2+}]_{free}/[OX^{2-}]_{free}$ ratio, we maintained constant free ionic calcium, $[Ca^{2+}]_{free}$, and free ionic oxalate, $[OX^{2-}]_{free}$, concentrations for the control and experimental solutions of corresponding RS values, achieving a virtually constant ratio for all solutions. This ratio also controls surface charging and the zeta potential of the COM surface [7,8], and may therefore influence crystal growth.

2. Materials and methods

Solution preparation. Reagent grade chemicals were used without further purification, and water of 10 MΩ conductivity was produced with a Milli-Q high purity water system. All solutions were filtered through 0.22 μm Millipore GS filters (4.7 cm diameter) and cation concentrations were determined with a Perkin-Elmer atomic absorption spectrophotometer. Calcium and oxalate concentrations were adjusted to achieve desired relative supersaturation (RS) values, with RS defined as the calcium-oxalate ion activity product divided by its equilibrium value. At each RS, two reactant solutions were prepared, one containing potassium oxalate and the other calcium chloride dihydrate. Typically, the buffered solution consisted of 0.1M sodium chloride, 0.01M HEPES, and determined levels of either potassium oxalate or calcium chloride dihydrate. The solutions were maintained at 37°C and pH was adjusted to 6.5. The total calcium and oxalate levels in each were chosen using EQUIL to ensure that uncomplexed Ca^{2+} was the same for samples with and without citrate. The second constraint in the EQUIL computations was to maintain the relative supersaturations of each pair of samples (i.e., with and without citrate). Calculated concentrations of free ionic and complex species for calcium oxalate monohydrate solutions in the presence and absence (values in parentheses) of citrate at a relative supersaturation of 19.7 (pH 6.5): total citrate, 3.5mM (none); sodium ion, 99.8mM (99.8mM); potassium ion, 1.60mM (1.88mM); calcium ion, 0.73mM (0.72mM); chloride, 106mM (102mM); oxalate, 0.51mM (0.49mM); citrate^{3-}, 1.17mM (none); HEPES (unprotonated), 1.34mM (1.33 mM); HEPES (protonated), 8.66mM (8.67mM); potassium chloride, 19.8μM (22.7μM); monohydrogen oxalate ion, 1.51μM (1.48μM); monosodium oxalate ion, 175μM (230μM); monopotassium oxalate ion, 0.044μM (0.052μM); calcium oxalate, 121μM (121μM); dicalcium oxalate ion, 6.27μM (6.18μM); calcium dioxalate ion, 1.06μM (1.02μM); calcium hydrogen oxalate ion, 0.021μM (0.021μM); monohydrogen citrate, 0.28mM (none); dihydrogen citrate, 2.05μM (none); monopotassium citrate, 6.65μM (none); calcium citrate anion, 2.02mM (none); calcium hydrogen citrate, 16.6μM (none). Between citrate-containing and control solutions, uncomplexed Ca^{2+} levels agreed within 1%, and uncomplexed Ox^{2-} within 4%; correspondingly, surface charge effects on COM due to variation in $[Ca^{2+}]_{free}$ were minimized.

Nucleation. A typical run began by rapidly mixing 2.5 mL each of the two reactant solutions by manually pushing the fluids through an in-line helical mixer into a 1 cm pathlength polystyrene

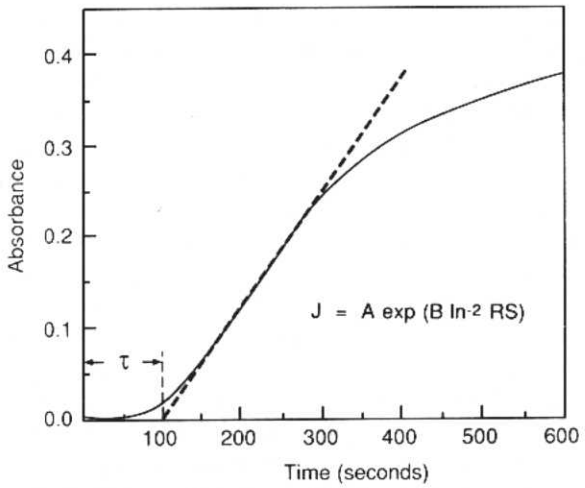

Fig. 1. Typical turbidity plot used for lag time measurements. RS 37 with 3.5mM citrate. $\tau = 100$ s.

cuvette. We chose polystyrene because glass, quartz, and acrylic cuvettes produced appreciable growth on their surfaces. Turbidity was measured for 10 min using a Perkin-Elmer 559A UV/VIS spectrometer in absorbance mode at 530 nm. Lag-times, τ, were determined from plots of absorbance versus time (fig. 1). The selected RS range was based on the behavior of turbidity measurements with respect to increasing RS. Below RS 20, the turbidity increase did not exceed 0.05 absorbance units, and lag-times resulting from small deviations above the baseline were considerably less certain. Above RS 37, lag-times were under 30 s. A typical experimental run is shown in fig. 1 where the dashed line indicates how the lag-time was evaluated by extrapolating to a turbidity value of zero; for example, in the case of citrate-containing systems at RS 19.7, the lag-time was 86 ± 17 s. This method gave reproducible estimates of the apparent nucleation lag-time. Therefore, we examined the dependence of τ on changes in the initial relative supersaturation of calcium oxalate. Apparent interfacial free energy, σ, was evaluated by plotting $\ln(1/\tau)$ versus $(\ln \mathrm{RS})^{-2}$ at six different relative supersaturation values to produce a linear plot (fig. 2); σ was obtained from the slope of the line as defined by the Gibbs–Thomson equation [9]:

$$J = A \exp\left(\frac{-16\pi\sigma^3 v^2}{3k^3T^3m^2[\ln(\mathrm{RS})]^2}\right),$$

where J is the nucleation rate which is proportional to $1/\tau$ (s^{-1}), A the pre-exponential factor, σ the apparent interfacial surface energy (erg cm^{-2}), v the molecular volume (for COM, 1.10×10^{-22} cm^3), k the Boltzmann constant (1.38×10^{-16} erg K^{-1}), T the absolute temperature (in these experiments, 310 K), m the number of growth units represented by v, and RS the relative supersaturation.

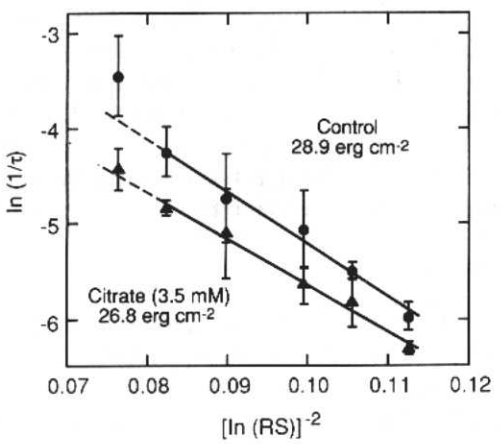

Fig. 2. Gibbs–Thomson nucleation plot: (●) control slope = -63 ± 6.3, intercept = 1.0 ± 0.60, $r^2 = 0.96$; (▲) 3.5mM citrate slope = -50 ± 1.9, intercept = 0.71 ± 0.18, $r^2 = 0.99$.

Crystal growth. COM seeds were produced using the dimethyl oxalate method [10]. First, a 2.5mM calcium chloride solution was prepared, and the pH adjusted to 4.7 with dilute ammonium hydroxide. Calcium chloride solution (150 mL) was added to 100 mL of ammonium acetate–acetic acid buffer (2.5 M with respect to each) into a 500 mL polymethylpentene plastic flask; then dimethyl oxalate (10 g) was added. The flask was tightly closed and heated in an oven at 90°C for 2.5 h, followed by rapid cooling to room temperature. Crystals were collected by centrifugation, washed with a RS 1 solution in NaCl–HEPES buffer, and diluted to 0.311 mg mL^{-1}. Crystals produced were monoclinic, with an average length of 3.5 μm (fig. 4c). The advantage of this method is that a substantial quantity of large morphologically well described crystals were pro-

duced by slowly generating oxalate in situ under zero-order kinetic conditions. Surface area of 1700 $cm^2\ g^{-1}$ was determined using the BET surface area analysis (Porous Materials, Inc.).

Equal volumes of calcium and oxalate reactant solutions were added to a 50 mL polymethylpentene flask maintained at 37°C in a water bath (^{14}C-oxalate was added as tracer to oxalate solutions). COM seed slurry (0.062 mg mL^{-1} final concentration) was added to initiate crystallization. At 5 min intervals, aliquots were removed and filtered through a 0.22 μm Nucleopore filter (25 mm). The filtrate was dispensed into a scintillation vial with 100 μL normal HCl and scintillation cocktail (Scintiverse II). Samples were counted using a Beckman LS 3801 liquid scintillation counter. The crystal-laden filters were also counted after rinses with 3 mL of RS 1 solution. Oxalate concentrations were determined, and RS values were calculated assuming a 1 : 1 calcium : oxalate precipitate. We should note that under these conditions [^{14}C] oxalate exchange with seeds should be negligible. To estimate the influence of citrate on the crystal growth rate of calcium oxalate monohydrate, we used the parabolic growth rate law: $(-\mathrm{d\,RS}/\mathrm{d}t = ks_t[\mathrm{RS}_t - \mathrm{RS}_\infty]^2)$. Integrating this equation gives

$$ks_t t = (\mathrm{RS}_t - \mathrm{RS}_\infty)^{-1} - (\mathrm{RS}_i - \mathrm{RS}_\infty)^{-1},$$

where t is the time interval from the beginning of crystallization (in seconds), RS_t the relative supersaturation at time t, RS_i the initial relative supersaturation, RS_∞ the relative supersaturation at equilibrium (defined as 1), K the crystal growth rate constant (s^{-1}), and s_t the total crystal surface area at time t. We calculated s_t by matching fractional changes in total seed mass as determined from the growth experiments to fractional changes in volume and correlated these to fractional changes in surface area using the surface area of the seeds (1700 $cm^2\ g^{-1}$) as s_0. Volume and surface were related to each other based on the geometry of hexagonal prisms closely similar in morphology and dimension to the actual seeds as observed by SEM.

Morphology. Samples for microscopic analysis were taken at specified intervals after beginning the experiment; typically, a 0.5 mL aliquot was removed and filtered through a 0.22 μm Nucleopore filter (13 mm). In the nucleation experiments, crystals were fixed after five and ten min for each of the twelve solutions. For the crystal growth experiments, crystals were filtered after 0, 3, and 24 h for RS 20 solutions with and without citrate. Crystals were then gold-coated and examined by scanning electron microscopy. Surface analysis was performed using a KEVEX X-ray spectrometer; no surface contaminants were found.

Particle characterization. Experimental systems the same as those used for lag-phase measurements were employed for purposes of particle characterization. Aliquots of these solutions were taken 20 min after mixing [11]. Total particle number and mode particle diameter (equivalent spherical diameter) were measured using an Elzone 80 XY (Particle Data, Inc.).

3. Results

To understand the action of citrate, we first applied a lag-phase kinetic analysis in which the appearance of crystals was evaluated turbidimetrically using a spectrophotometer at a non-absorbing wavelength (530 nm). When data collected in these experiments were analyzed using the Gibbs–Thomson equation as discussed above, plots of $\ln(1/\tau)$ versus $(\ln \mathrm{RS})^{-2}$ gave slopes of -62.5 ± 1.92 for control and -49.5 ± 6.26 for the experiment with citrate; intercepts were 1.03 ± 0.2 and -0.72 ± 0.6 respectively. The slopes were further analyzed by converting them into values for the apparent interfacial energy for nucleation. This was done by solving the equation

$$\mathrm{slope} = (-16\pi\sigma^3 v^2/3k^3T^3), \qquad (2)$$

taken from the linearized form of the Gibbs–Thomson equation (cf. eq. (1)). Apparent interfacial energy for the control was 28.9 erg cm^{-2}, and for the citrate system it was 26.8 erg cm^{-2}. These values may be compared with those derived for systems very similar to our control system. In earlier work [1], we found a value of 27.3 erg

cm^{-2}, and Finlayson [11] gave the value 31.1 erg cm^{-2}.

As another way of looking at nucleation, we examined particle production in our nucleating systems. Based on the observations of Finlayson [11], we expected total particles, N, to be a rather flat and somewhat noisy function of relative supersaturation in this range of RS. This proved to be the case, however, we did detect statistically significant differences in N and in equivalent spherical diameter between the control and citrate systems. Without citrate, the nucleating systems produced an average of $3.46\ (\pm 1.94) \times 10^7$ particles per liter, with an average mode diameter of $12.4 \pm 3.8\ \mu$m. With citrate, N was $7.14\ (\pm 2.78) \times 10^7$ particles per liter, with an average mode diameter of $8.2 \pm 1.3\ \mu$m.

Although there was a relatively small but significant difference between the apparent interfacial energies of the control and experimental systems, there was a considerable difference between the lag-times in the two sets of solutions at corresponding relative supersaturations. Table 1 shows that lag-times in citrate systems were invariably longer than the control systems by an average of 75%. We believed that the interfacial energies were an accurate reflection of nucleation in our experiments, and that the discrepancy in lag-times could be explained by growth inhibition due to the presence of citrate.

Crystal growth studies did indeed show a significant difference in growth rates at a citrate concentration of 3.5mM (see fig. 3). Again, we sought to control the solution very closely so that differences in crystal growth rates could be clearly attributed to citrate. The surface normalized crystal growth rate in the control was $2.36\ (\pm 0.16) \times 10^{-6}\ s^{-1}\ cm^{-2}$, whereas for the citrate system it was $0.66\ (\pm 0.03) \times 10^{-6}\ s^{-1}\ cm^{-2}$. The reduced growth rate of COM in the presence of citrate allowed us to explain the differences in particle counts and sizes we had observed. It was clear that growth inhibition would cause smaller particles as we had seen with citrate, but because growth was delayed, the relative supersaturation, and therefore the nucleation rate, did not fall as quickly, consequently, more particles were produced. Taken by itself, the doubling of the lag-times with citrate might have been interpreted as inhibition of nucleation while the doubling of the particle counts might have been interpreted as promotion of nucleation. By bringing several techniques to bear on this closely controlled experimental design, a self-consistent view of the action of citrate emerged which explained these apparently conflicting results.

As in our previous report on nucleation, we attempted to model these results with our crystallization simulation program, PSD [1,12]. These efforts are still in the preliminary stages, but early

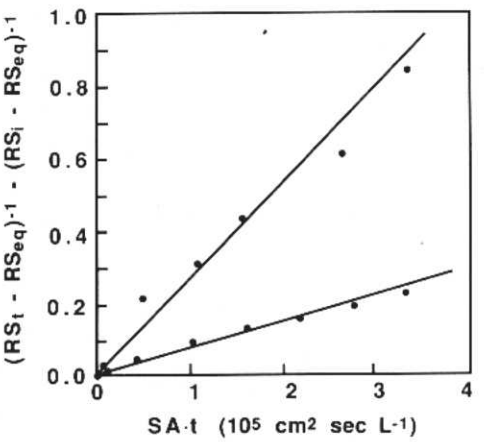

Fig. 3. Determination of crystal growth rates: (●) control, $K = 4.7 \pm 0.33 \times 10^{-5}\ cm^2\ s^{-1}$, intercept $= 0.093 \pm 0.052$, $r^2 = 0.98$, $N = 7$; (▲) 3.5mM citrate, $K = 1.1 \pm 0.10 \times 10^{-5}\ cm^2\ s^{-1}$, intercept $= 0.068 \pm 0.018$, $r^2 = 0.96$, $N = 7$.

Table 1
Kinetics of calcium oxalate monohydrate nucleation in the absence and presence of 3.5mM citrate [a]

Relative supersaturation	Observed lag times (s)	
	Control	3.5mM citrate
20	400±44	560±26
22	250±14	350±80
24	170±66	290±47
28	130±57	170±61
33	70±19	140±33
37	30±12	90±17

[a] Note that the uncomplexed calcium ion concentrations for each pair of control and citrate samples were the same, based on calculations with EQUIL.

results are encouraging because the simulations do reflect the general trends of the experiments.

The effect of citrate was seen in a striking way in electron micrographs of crystals from the nucleating systems. Fig. 4a shows crystals of COM nucleated in the control system. These crystals had a characteristic morphology for COM; they were twinned (as in fig. 4c) and had a prominent elongated hexagonal face. In the presence of citrate, however, the crystals were broader and flatter with an aspect similar to regular hexagons (fig. 4b). Seed crystals used in seeded growth experiments (fig. 4c) were not altered much in shape by either control systems (fig. 4d) or systems containing citrate (figs. 4e and 4f).

4. Discussion

In evaluating the inhibitory action of citrate, we found that compensation for the complexation of cations made a very considerable difference in the observed nucleation and growth rate behavior. To achieve equal uncomplexed calcium ion concentrations in the absence and presence of citrate, the total calcium concentration had to be raised significantly. In the control samples, uncomplexed calcium ion corresponded to about 85% of the total calcium ion concentration, whereas it was only 25% of total calcium in the presence of citrate. Failure to account for the importance of complexation would have resulted

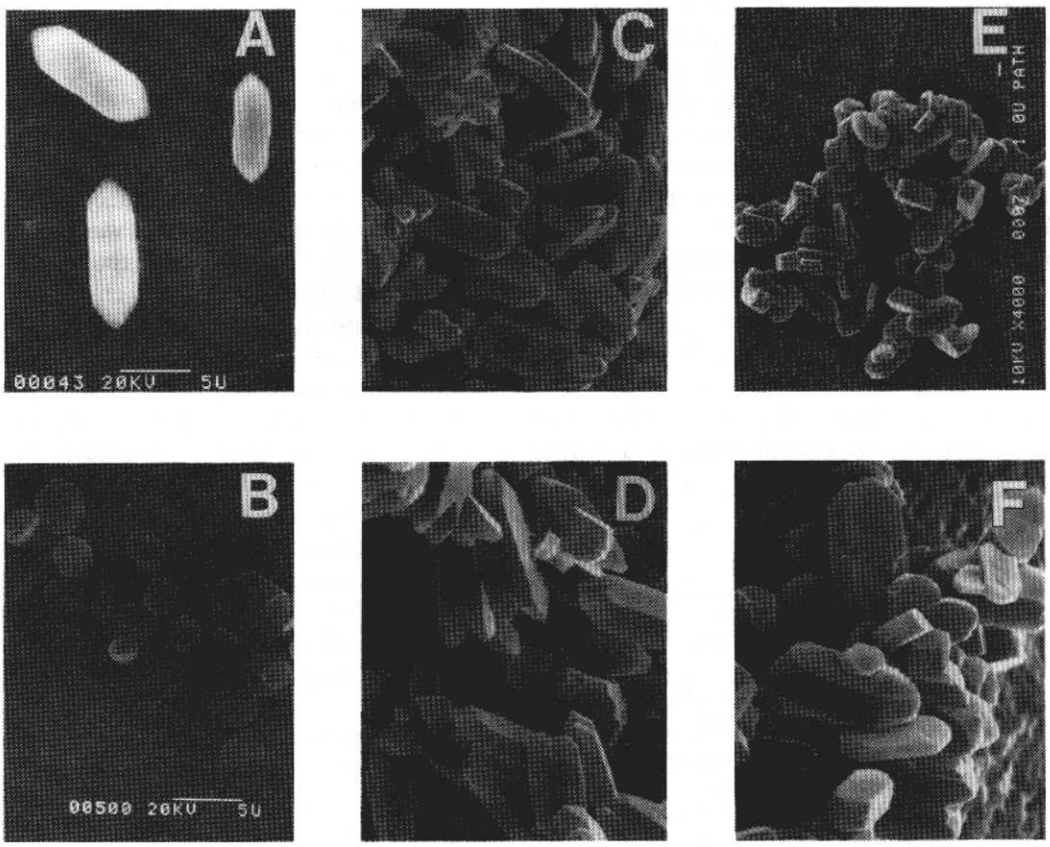

Fig. 4. Photographs of COM using scanning electron microscopy. Nucleation experiments at 10 min: (a) RS 20 control; (b) RS 20 with 3.5mM citrate. Crystal growth experiments: (c) COM seeds at time zero; (d) COM seeds grown for 3 h in RS 20 control solution; (e) COM seeds grown for 3 h in an RS 20 containing 3.5mM citrate solution (magnification: 4000×); (f) COM seeds grown for 3 h in RS 20 containing 3.5mM citrate solution (magnification: 7800×).

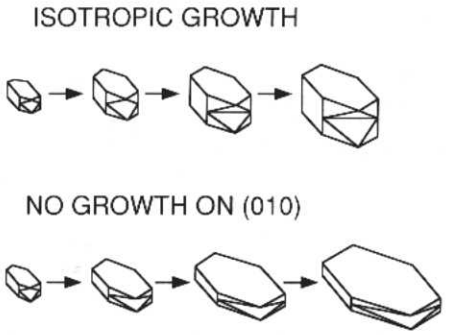

Fig. 5. Computer simulation of COM crystal growth. (a) Morphology of control crystal as predicted by maturing each crystal face. Initial "nucleus" has an identical morphology. (b) Morphology of crystal computer grown in a 3.5mM citrate solution by restricting growth on (010) face. See fig. 4b.

in misleading inferences about apparent differences in the kinetics of nucleation and crystal growth. By using EQUIL, however, we could correct for these chelation effects by citrate, and our data show that the presence of calcium citrate complex and citrate ions resulted in about a 70% decrease in crystal growth rate. This observation indicates that uncomplexed citrate and/or calcium citrate must reduce the efficiency of adding calcium ion, oxalate ion, or calcium oxalate complex to crystal growth sites.

From our kinetic and morphological studies of calcium oxalate monohydrate crystals, we now propose that citrate adsorbs preferentially to one crystal face, thereby altering the morphology of the crystals during the further accretion of calcium oxalate into the crystal. As shown in fig. 5, we could start with a common initial crystal morphology and allow crystals to "grow" using a computer program that represented changes in crystal mass as a change in total volume of the geometrically defined crystal. Without any change in apparent rates of addition to the various crystal faces, morphology was maintained; however, by restricting growth on the (010) face, increased addition to the other faces resulted in hexagonal plates shown in this figure. Using the X-ray crystallographic data of Deganello and Piro [13] we developed a specific proposal regarding this binding behavior. Of the three major planes defining the calcium oxalate monohydrate crystal (i.e., the (010), ($\bar{1}$01), and the (001) planes), only the first two have oxalate groups parallel to the face, and citrate would most probably replace oxalate ion by binding on the ($\bar{1}$01) face. In any case, the morphological changes due to the adsorption of citrate may be significant in urolithiasis, because crystal–cell interactions and crystal aggregation processes are both likely to be influenced by changes in crystal morphology. For example, Wiessner et al. [14] reported that COM crystals exhibit a much higher capacity to cause red blood cell membranolysis than do dihydrate crystals. Likewise, the adhesion of COM crystals to papillary cells are likely to be affected by the contour and nature of the various faces of calcium oxalate crystals. Crystal aggregation may also depend upon morphology, and the hexagonal plates formed in the presence of citrate may aggregate more readily. All of these considerations have led us to initiate a longer term study using stereochemical considerations as the basis for molecular recognition at crystal interfaces [15]. Such efforts have already provided many valuable inferences regarding changes in crystal morphology arising from face-specific interactions of crystals and growth inhibitors [16,17]. While clearly beyond the scope of our present work on citrate, we are attracted by the potential of the molecular recognition approach which may reveal how low-molecular-weight inhibitors such as citrate and pyrophosphate, as well as macromolecules (e.g., nephrocalcin and Tamm–Horsfall proteins) affect crystal growth processes.

Finally, although nucleation and growth processes in the case of calcium oxalate monohydrate appear to overlap during the initial lag-phase of precipitation, our earlier studies [1] as well as those of Söhnel and Mullin [18] indicate that such lag-phase kinetics can be treated phenomenologically in terms of the Gibbs–Thomson formulation. Nevertheless, as we probe further into the details of the early steps in COM crystallization using the tools of molecular recognition theory to establish a structural perspective, we recognize that more advanced theoretical treatments of precipitation could be helpful. Such models might, for example, allow for the deconvolution of the overlapping time domains of nucleation and growth steps.

References

[1] C.M. Brown, D.K. Ackermann, D.L. Purich and B. Finlayson, J. Crystal Growth 108 (1991) 445.
[2] I. Greenwald, J. Biol. Chem. 124 (1938) 437.
[3] B. Kissen and M.O. Locks, Soc. Expt. Biol. Med. Proc. 46 (1941) 216.
[4] I.S. Light and H.H. Zinsser, Arch. Biochem. Biophys. 92 (1961) 487.
[5] H. Sidhu, R. Gupta, S. Thind and R. Nath, Urol. Res. 14 (1986) 299.
[6] P. Werness, C. Brown, L. Smith and B. Finlayson, J. Urol. 134 (1985) 1242.
[7] P. Curreri, G.Y. Onoda and B. Finlayson, J. Colloid Interface Sci. 69 (1978) 170.
[8] J.H. Adair, Coagulation of Calcium Oxalate Monohydrate Suspensions, PhD Dissertation, University of Florida, Gainesville, FL (1981).
[9] A.G. Walton, The Formation and Properties of Precipitates (Kreiger, Huntington, NY, 1979) pp. 3–7.
[10] L. Gordon, M.L. Salutsky and H.H. Willard, Precipitation from Homogeneous Solution (Wiley, New York, 1959) pp. 57–58.
[11] B. Finlayson, Kidney Intern. 13 (1978) 344.
[12] B. Finlayson, Comment on the round table discussion on theoretical models related to urolithiasis, in: Urolithiasis and Related Clinical Research, Eds. P.O. Schwille, L.H. Smith, W.G. Robertson and W. Vahlensieck (Plenum, New York, 1985) pp. 923–933.
[13] S. Deganello and O.E. Piro, Neues Jahrb. Mineral. Monatsh. H 2 (1981) 81.
[14] J.H. Wiessner, G.S. Mandel and N.S. Mandel, J. Urol. 135 (1986) 835.
[15] I. Weissbuch, L. Addadi, M. Lahav and L. Leiserowitz, Science 253 (1991) 637.
[16] J.D. Foot and E.A. Colbourn, J. Mol. Graphics 6 (1988) 93.
[17] I. Weissbuch, L. Addadi, L. Leiserowitz and M. Lahav, J. Am. Chem. Soc. 110 (1988) 561.
[18] O. Söhnel and J. Mullin, J. Colloid Interface Sci. 123 (1988) 43.